Hindawi
Advances in Polymer Technology
Volume 2023, Article ID 7343992, 11 pages
https://doi.org/10.1155/2023/7343992

Research Article

Equibiaxial Planar Tension Test Method and the Simulation Analysis for Hyperelastic EAP Membrane

Huaan Luo,[1] **Yinlong Zhu**,[2] **Haifeng Zhao**,[1] **Luqiang Ma**,[1] **and Jingjing Zhang**[1]

[1]*School of Intelligent Manufacturing, Nanjing Vocational College of Information Technology, Nanjing, China*
[2]*College of Mechanical and Electronic Engineering, Nanjing Forestry University, Nanjing, China*

Correspondence should be addressed to Huaan Luo; luoha@njcit.cn

Received 30 September 2022; Revised 11 April 2023; Accepted 18 April 2023; Published 19 May 2023

Academic Editor: Gyorgy Szekely

The equibiaxial planar tension test is an important method for determining the mechanical properties of hyperplastic membranes, and it is also critical to designing an effective equibiaxial tension test rig to meet experimental accuracy requirements. However, any analysis addressing the accuracy of this test is not reported in the literature. In this paper, an equibiaxial planar tension apparatus is proposed for conducting single-corner-point tension tests on hyperelastic electroactive polymer (EAP) membranes. The experimental data were compared with those obtained from two-corner-point-fixed tension tests and fitted with nonlinear material models, and the model's parameters were also evaluated. Finally, the widely-used finite element software ABAQUS was employed to simulate equibiaxial planar tension methods and investigate the impact of clamping mode and point number on test accuracy as well as the uniformity of overall deformation. The test results indicate that the stress-strain curves for the two tensions remain consistent across small stretch ratios. However, as the stretch ratio increases (about $\lambda > 2.25$) in two-corner-point-fixed tension, stress shielding may lead to a degradation of strain uniformity and result in greater stresses than single-corner-point tension. Additionally, both the three-parameter Yeoh model and the four-parameter Ogden model can provide an accurate description of the EAP membrane material. The simulation results indicate that the axial strain variation amplitudes remain below 5% within a region spanning approximately 80% of the specimen's overall length from its center to edge and even below 1% within a region spanning 85% in the single-corner-point tension; stress inaccuracies increase with stretch ratio, while the calculated error is about 2.1% when $\lambda = 4$ in the single-corner-point tension test, which has the smallest stress error among the tests; when the number of tension points is increased, the overall deformation becomes more sufficient, and the test accuracy improves as well. The conclusions drawn from this paper will be beneficial in designing equibiaxial planar tension test rigs and analyzing their accuracy and uniformity of deformation.

1. Introduction

The hyperelastic membrane material represented by EAPs possesses the characteristics of large elasticity and high strain energy density. It has a wide application prospect in high-tech fields such as soft robots [1–3], flexible actuators, and transducers [4, 5]. Because the uniaxial tension test cannot accurately describe such material characterization and because friction between the contact surfaces occurs during uniaxial compression, resulting in complex stress states such as compression and shear, which results in inaccurate test results, the equibiaxial tension test of a hyperelastic membrane has become the primary method for determining its mechanical properties. [6–8]. Typical equibiaxial tension test methods include a square specimen equibiaxial planar tension test (Figure 1(a)), a radial tension test (Figure 1(b)), and a circular specimen expansion test (Figure 1(c)) [9–13]. Figure 1 depicts the ideal tensile principle. Among these, equibiaxial planar tension is widely used for hyperelastic membrane material tests due to its ease of use and controllability.

Equibiaxial planar tension first appeared in the mechanical property test of soft tissue materials such as rabbit skin [14, 15]. Such kind of materials have little strain, and the samples generally need to be pretreated. Another application field of the equibiaxial planar tension test involves hyperelastic polymer membrane materials such as rubber [9, 15–17].

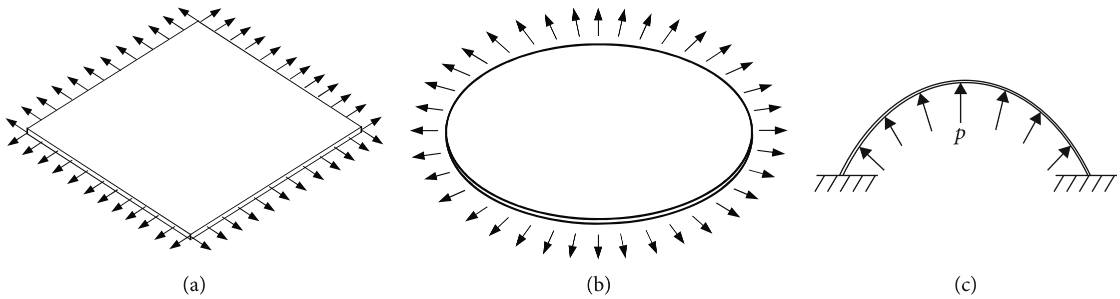

FIGURE 1: Typical equibiaxial tension tests: (a) equibiaxial planar tension, (b) radial tension, and (c) bulge test.

In the equibiaxial planar tension test, nonuniformity deformation near the corner will affect the accuracy of the test [18]. Therefore, Obata et al. modified the clamping condition of the corner chucks to minimize the nonuniform deformation of the specimen [19]. Blatz et al. added clips at four corner points of the square membrane specimen for clamping and stretching [20, 21]. In some simple test rigs, the fixture blocks are also used for clamping in tension tests, but there will exist serious stress concentration and stress shielding [22, 23]. Despite the widespread use of various equibiaxial planar tension test methods, no comparative analysis of these test methods as well as their accuracy has been published.

The finite element method (FEM) has become extensively used to design and optimize products or complex processes because it reduces the number of physical prototypes and experiments required during the design cycle. Experimental modal analysis (EMA) for rubber supports [24] and modeling a skin-pass rolling process to predict experimentally difficult-to-measure variables [25] are two examples. There is no doubt that the FEM is a viable approach to evaluating the equibiaxial tension test method [26].

It is assumed that the energy stored in hyperelastic materials depends solely on their initial and final states of deformation, which are independent of the path of deformation or load. Therefore, strain energy density functions (SEDFs) are commonly used to characterize hyperelastic materials such as rubber-like materials [9, 10, 19, 20], various hydrogels, and their composite [27, 28]. EAP is a kind of high-molecular polymer with viscoelasticity, and its nonlinear behavior can also be better described by SEDFs [17].

This work developed a multifunctional equibiaxial planar tension test rig coupling with a machine vision system to conduct a single-corner-point equibiaxial planar tension test to study the nonlinear stress-strain behavior of hyperelastic EAP materials. The experimental results were also compared with those from the two-corner-point-fixed tension method. Through the finite element software ABAQUS, the two equibiaxial planar tension methods were modeled, the simulation for the multipoint tension with two-corner-point-fixed was also carried out, and their results were compared with that from the theoretical calculation. Finally, to understand the overall non-uniform deformation of equibiaxial planar tension, tensile efficiency was also analyzed. The findings of this paper will be useful in designing test rigs and analyzing the accuracy of equibiaxial planar tension.

2. Experimental Section

2.1. Constitutive Model of Hyperelastic Membrane Based on Equibiaxial Tension. For hyperelastic materials, various types of SEDFs can be utilized to characterize their properties. This paper investigates three typical constitutive models: Mooney-Rivlin [29, 30], Yeoh [31], and Ogden [32].

2.1.1. Mooney-Rivlin Model. For incompressible materials, the SEDF can also be considered as a function of two strain invariants

$$W = \sum_{k+l=1}^{N} C_{kl}(I_1 - 3)^k (I_2 - 3)^l, \quad (1)$$

where C_{kl} is the Mooney-Rivlin material parameter and N is the model order. In practical application, the first order with two terms of its power series is usually taken, i.e.,

$$W = C_{10}(I_1 - 3) + C_{01}(I_2 - 3). \quad (2)$$

Here, I_1 and I_2 are the strain invariants of the Cauchy-Green deformation tensor, determined by the stretch ratios λ_i ($i = 1$, 2, and 3) in three principal directions, and the stretch ratio is the ratio of the geometric dimension after stretching to the original one of the specimen in principal directions:

$$\begin{aligned} I_1 &= \lambda_1^2 + \lambda_2^2 + \lambda_3^2, \\ I_2 &= \lambda_1^2\lambda_2^2 + \lambda_2^2\lambda_3^2 + \lambda_3^2\lambda_1^2. \end{aligned} \quad (3)$$

2.1.2. Yeoh Model. In the formula of Mooney-Rivlin, if only term I_1 is partially expanded, the typical third-order Yeoh SEDF can be obtained

$$W = C_{10}(I_1 - 3) + C_{20}(I_1 - 3)^2 + C_{30}(I_1 - 3)^3 \quad (4)$$

2.1.3. Ogden Model. Ogden removed the restriction that the function is an even power of the stretch ratio and proposed an SEDF in the series form

$$W = \sum_{k=1}^{N} \frac{\mu_k}{\alpha_k}\left(\lambda_1^{\alpha_k} + \lambda_2^{\alpha_k} + \lambda_3^{\alpha_k} - 3\right), \quad (5)$$

where μ_k and α_k are the material parameters. In some works of literature [10, 17], the above-mentioned Ogden SEDF usually takes another form

$$W = \sum_{k=1}^{N} \frac{2\mu_k}{\alpha_k^2} \left(\lambda_1^{\alpha_k} + \lambda_2^{\alpha_k} + \lambda_3^{\alpha_k} - 3 \right). \quad (6)$$

This formula is also used in the finite element analysis software ABAQUS. It is the same as the original formula with only a formal difference. For incompressible materials, with the relation $\lambda_1 \lambda_2 \lambda_3 = 1$, SEDFs can be simplified.

According to SEDFs, the principal Cauchy stress σ_i (i =1, 2, and 3) can be derived:

$$\sigma_i = \lambda_i \frac{\partial W}{\partial \lambda_i} - P_h, \quad (7)$$

where P_h is the hydrostatic pressure, which is determined by the dynamic boundary condition. According to $\sigma_3 = 0$, the expressions of the stress in two principal directions under the condition of equibiaxial tension can be deduced

$$\sigma = \sigma_1 = \sigma_2 = \lambda_1 \frac{\partial W}{\partial \lambda_1} - \lambda_3 \frac{\partial W}{\partial \lambda_3}. \quad (8)$$

Under the assumption of incompressibility and isotropy, $\lambda_1 = \lambda_2 = \lambda$ and $\lambda_3 = 1/\lambda^2$, the equibiaxial tension stress σ can be derived. When the SEDF of Yeoh or Mooney-Rivlin is used, Equation (8) can also be rewritten directly in terms of I_1 and I_2 as

$$\sigma = 2\left(\lambda^2 - \lambda^{-4}\right) \left(\frac{\partial W}{\partial I_1} + \lambda^2 \frac{\partial W}{\partial I_2} \right). \quad (9)$$

Substituting the above-mentioned SEDFs into Equation (8) or Equation (9), the stress formula for different models of equibiaxial tension can be obtained. In general, the relationship between engineering stress S and stretch ratio λ is used to express the stress-strain relationship of hyperelastic materials where S equals Cauchy stress (also known as real stress) divided by λ:

$$S = \frac{\sigma}{\lambda}. \quad (10)$$

The EAP membrane material analyzed in this paper is VHB4910 from 3M™, a commercial double-sided adhesive tape that belongs to the acrylic polymer family and is widely used to manufacture flexible actuators and transducers due to its good deformation capacity when subjected to the action of an electric field.

2.2. Equibiaxial Planar Tension Test. Equibiaxial planar tension is a method that generates equibiaxial planar deformation by applying uniform tensile force (or displacement) to the periphery of a square membrane specimen (Figure 1(a)). In practical applications, there are various methods that can be used to secure the square specimen. These include using small staples hooked along its edges [14], inserting silk threads into uniformly spaced holes on each side of the specimen [9], and utilizing clamping clips [15] or self-tightening chucks of a special tensile tester [19]. This study involves EAP square membrane specimens, and a uniformly distributed multipoint tension method (Figure 2) was designed to reduce stress concentration and stress shielding phenomena [22, 23]. The clips were chosen to secure the four edges of the specimen while minimizing the clamping area as much as possible.

2.2.1. Test Method. In an ideal condition, uniformly distributed loads are applied by the clips along the four edges of the specimen to conduct equibiaxial free tension, where the tangential displacements of the tensile points are not constrained. Due to the resistance friction that exists when the clips move and the tensile points near the corner cannot provide enough tension to realize lateral "fast" movement of other points, the specimen can easily be torn when the stretch ratio becomes large enough. Therefore, the two-corner-point-fixed tension method is employed, wherein the distance between two clamping points on mutually perpendicular edges adjacent to the corner remains constant during the extension process [18], as depicted in Figure 2(a).

If only the two adjacent points to the corner are fixed during extension, the strain between the points of the specimen remains constant, resulting in stress shielding. Meanwhile, excessive deformation will occur near the membrane specimen's corner, resulting in the membrane being torn and the loss of experimental accuracy. A single-corner-point tension method may be employed to improve deformation uniformity in the corner area, in which the connecting bar between the two points near the corner in Figure 2(a) is removed and four additional clips are added at each corner (Figure 2(b)) of the specimen, and concentrated forces (or displacements) at 45° to the tensile direction are exerted at the corner points (clips) when equibiaxial planar tension is conducted.

It is simple to calculate the stress and strain of equibiaxial planar tension. Measuring and recording the total tensile force F in the principal direction, then divided by the original sectional area A_0 of the square membrane, the nominal stress S can be obtained, i.e.,

$$S = \frac{F}{A_0} = \frac{F}{(L_s t_0)}, \quad (11)$$

where L_s is the initial length of the square membrane specimen and t_0 is the original thickness. According to the manufacturer's instructions, the thickness of membrane VHB4910 is 1 mm. The strain can be calculated or detected based on their measured displacement or deformation of the testing marks in Figure 2. To collect deformation data continuously, the machine vision system is adopted to measure the deformation of the rectangular mark in Figure 2(b).

2.2.2. Test Rig. Due to the uneven deformation near the corners that exist in the two-corner-point-fixed equibiaxial planar tension [18], a multifunctional equibiaxial planar tension test rig based on single-corner-point tension was

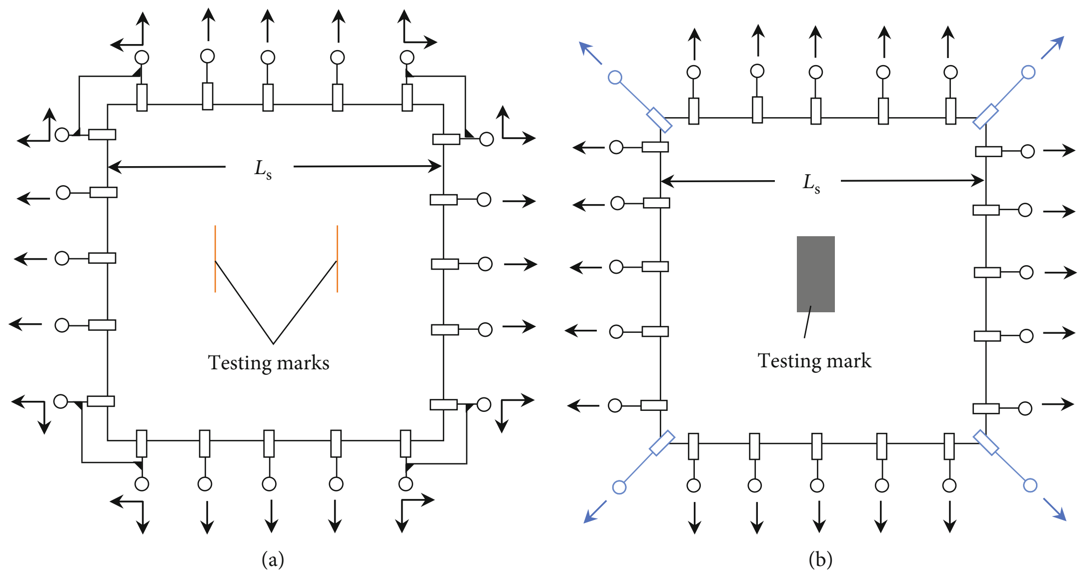

Figure 2: Equibiaxial planar tension tests: (a) two-corner-point-fixed tension and (b) single-corner-point tension. Testing mark(s) are preprinted on the specimens, and the strain can be calculated or detected based on their measured displacement or deformation.

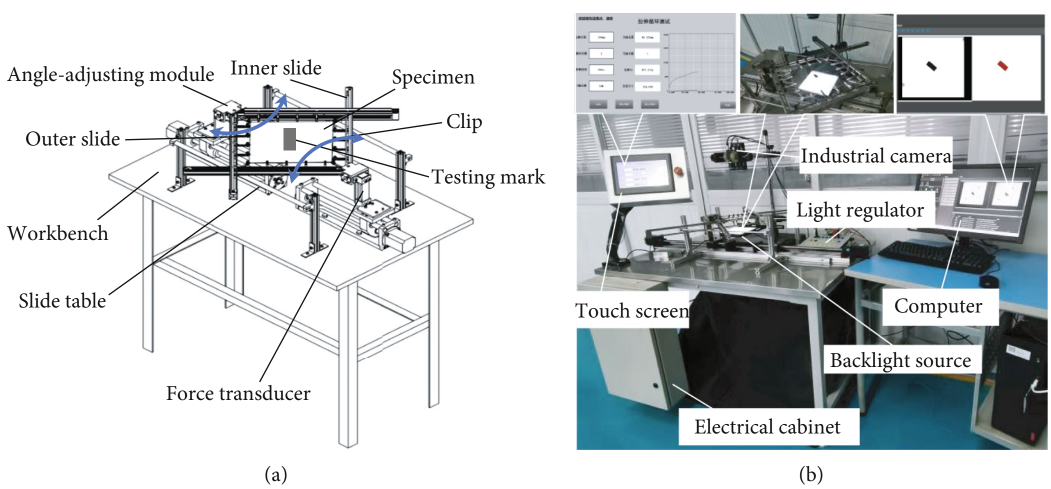

Figure 3: A multifunctional equibiaxial tension test rig: (a) schematic drawing of the main structure and (b) picture of the test rig.

specially developed (Figure 3). The rig mainly consists of a workbench, inner slide, outer slide, slide tables, angle-adjusting modules, and force transducer. Two slide tables are symmetrically mounted on the workbench. Two stepper motors on the tables drive the lead screws, leading the inner and outer slides to reciprocate, respectively, along the axial direction to conduct the tension test of hyperelastic membrane materials.

The designed key structure of the test rig lies in a pair of 90° V-shaped inner and outer slides that can adjust the angle along the tensile direction, and two arms of the slide cross each other at 90°. The arms of the inner slide are inserted into the rectangular holes of the outer slide which provide guidance and support. Up to twenty clips equipped with rollers at each rear end clamp the specimen edges and can move along the slide grooves. Two clips are fixed at the corner of the slide, and the other two clips located at the intersection of the two slides can move along the two grooves simultaneously. The angle-adjusting module (Figure 3(a)) mainly consists of a worm gear mechanism, arranged at the end of the slide, which can adjust the swing angle to fulfill biaxial tension. The test rig is characterized by a compact uniaxial structure to realize biaxial tension.

The membrane specimen is clamped by the clips along each edge, including four corners. The clamping points are uniformly distributed, and the tensile force is measured by a force transducer installed at the rear end of the slide (Figure 3(a)). The stepper motors are controlled by a PLC (programmable logic controller) installed inside the electrical cabinet. The analog signal module of the PLC is responsible for collecting the tensile data from the force transducer and the human-machine interaction realized by the touch screen. The strain is obtained by measuring the deformation of the rectangular testing mark on the surface of the

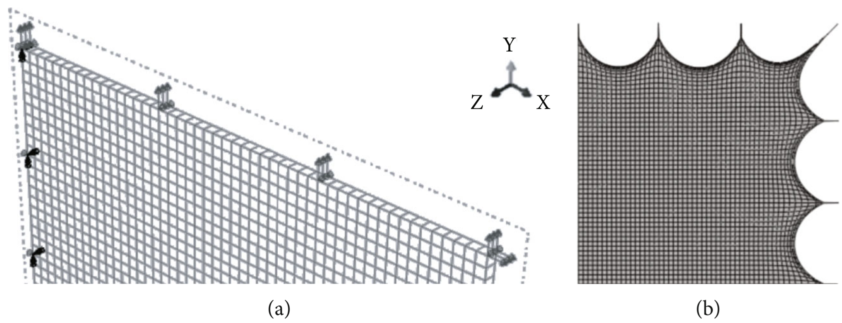

Figure 4: FEM simulation of single-corner-point equibiaxial planar tension on square specimen: (a) scheme of the model and (b) deformed shape after tension.

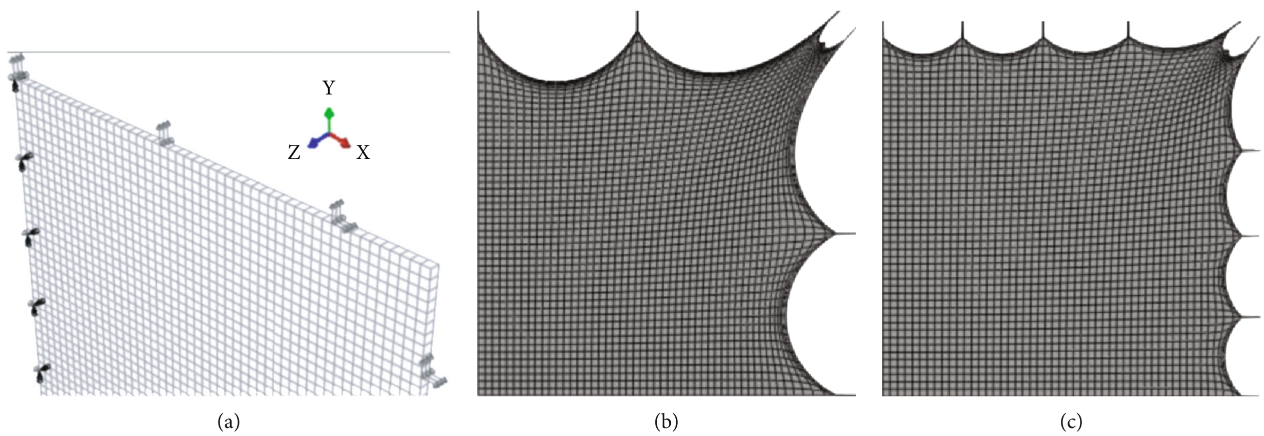

Figure 5: FEM simulation of two-corner-point-fixed equibiaxial planar tension: (a) scheme of the model and (b) deformed shape of the tension with five points along one edge, and (c) deformed shape of the multipoint tension with nine points along one edge.

specimen with the help of the machine vision system, which mainly consists of an industrial camera, backlight source, light source regulator, and computer. The computer collects the deformation data of the mark and the tensile forces simultaneously for calculation and analysis (Figure 3(b)).

2.3. Simulation Analysis for the Tension Tests. The experimental accuracy and other performances need to be examined because the results of the tests listed above may differ. When combined with a relatively limited number of experimental data, FEM can be used to evaluate material models and adjust their constants that are most appropriate for modeling the material behavior [33–35] and to vary the specimen parameters and loading modes to research the failure mode of material conveniently [36]. This provides a quick, simpler, and more economical alternative method to study material characterization. In this paper, ABAQUS was used to evaluate whether the results of the equibiaxial planar tension methods are in good agreement with the theoretical result of a standard square membrane suffering equibiaxial planar tension.

The FE model of the hyperelastic membrane has identical geometry and dimensions to that of the actual specimen. In order to reduce computational cost, a quarter of the specimen was utilized with symmetry conditions imposed on the left and lower planes for modeling equibiaxial planar tension tests on standard square EAP membranes. To facilitate the convergence of the model for simulating practical equibiaxial tension tests, the tension mode was simplified. The ramp displacements were eventually applied to the uniformly distributed lines instead of clips after evenly partitioning the upper and right planes of the specimen into several regions (Figure 4). The model was meshed using three-dimensional eight-node hybrid solid elements (C3D8H). The mesh seeding was controlled with an approximate global size and verified, resulting in a total of 2500 elements. The Ogden model is used in this work, and the material parameters of the EAP membrane are taken from the literature [17].

The experimental accuracy will vary depending on the equibiaxial planar tension method used. Moreover, the deformation uniformity will fluctuate depending on how many clamping points are used in the test. Other tension methods, such as two-corner-point-fixed tension and multipoint tension of two-corner-point-fixed tension, were also simulated in addition to the single-corner-point equibiaxial planar tension method.

Once the boundary conditions for the square specimen have been defined, displacement loads can be applied to the tensile points. In the single-corner-point tension (as illustrated in Figure 4), a 45° displacement direction was set for the corner's tensile point relative to the tensile direction, resulting in two perpendicular and equal displacements

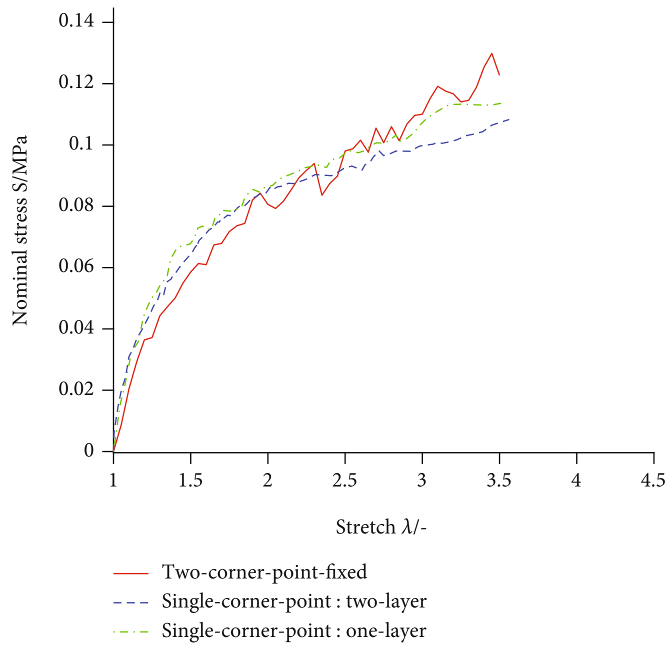

FIGURE 6: Comparison among the results of various equibiaxial planar tension tests.

being applied to this point. In the two-corner-point-fixed tension, the distance between two clips clamped on perpendicular edges and close to the corner must remain constant during stretching. Therefore, two pairs of equal and perpendicular displacements are applied to those points (see Figure 5). The tensile points were increased in the multipoint tension (Figure 5(c)) based on the two-corner-point-fixed tension. Other points in the equibiaxial planar tension were free of tangential except for the corner point and the points along the symmetry axis. The axial tensile force F is calculated in the simulation by adding the tensile forces f_n at each tensile point ($n = 1, 2,..., N_P$, where N_P is the total number of tensile points along the edge), and the tensile forces near or at the corner are taken from their force component.

3. Results and Discussion

The equibiaxial tension tests mentioned above were conducted on a horizontal plane. One-layer and two-layer membranes with identical geometric dimensions were selected as specimens for the tests to account for experimental inaccuracies resulting from structural bending moments, manufacturing errors, friction between moving parts, and other factors. The accuracy of experimental data can be verified by comparing and analyzing the impact of system errors in the test rig. The one-layer square membrane has geometric dimensions of 100 mm × 100 mm × 1 mm, while the two-layer membrane specimen consists of two laminated one-layer membranes. The specimens were stretched at an extremely low speed ($\dot{\lambda} \approx 5 \times 10^{-4}$ s^{-1}) to satisfy quasistatic conditions. Because the force transducer is positioned at the corner of the 90° V-shaped slide, the tensile force F in Equation (11) is equivalent to the measured tensile force multiplied by the coefficient of $1/\sqrt{2}$.

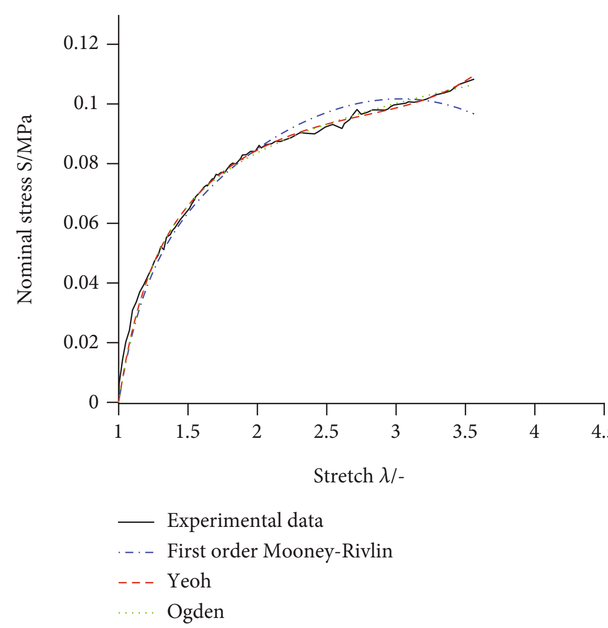

FIGURE 7: Hyperelastic models vs. experimental data of equibiaxial planar tension.

3.1. Analysis of Experimental Results. Based on experimental data, the stress-strain curves (S-λ) were calculated and presented in Figure 6, which includes both one-layer and two-layer equibiaxial single-corner-point planar tension data. Additionally, the stress-strain curve obtained from a two-corner-point fixed tension test was also included for comparison [37].

It can be seen from Figure 6 that the behavior curves obtained from one-layer and two-layer specimens utilizing the single-corner-point tension method exhibit minimal deviation, indicating negligible system error during testing.

Table 1: Material parameters in three hyperelastic models.

Model		Parameters		RMS/-	
		Two-corner-point-fixed tension	Single-corner-point tension	Two-corner-point-fixed tension	Single-corner-point tension
Mooney-Rivlin	C_{10}/MPa	2.19E-2	2.53E-2	3.37E-3	3.42E-3
	C_{01}/MPa	-3.50E-4	-9.21E-4		
Yeoh	C_{10}/MPa	2.16E-2	2.56E-2	3.17E-3	1.76E-3
	C_{20}/MPa	-1.24E-4	-4.58E-4		
	C_{30}/MPa	1.00E-6	6.85E-6		
Ogden	μ_1/MPa	4.03E-2	1.43	3.22E-3	1.91E-3
	α_1	1.81	-1.65		
	μ_2/MPa	7.16E-1	-1.47		
	α_2	1.69E-2	-1.75		

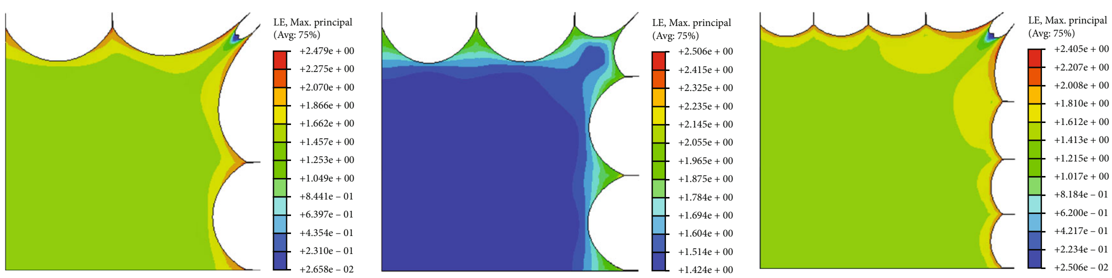

(a) (b) (c)

Figure 8: Strain contour maps in equibiaxial planar tension test: (a) two-corner-point-fixed tension, (b) single-corner-point tension, and (c) multipoint tension with two- corner-point-fixed.

Although the stresses of the one-layer specimen abnormally increased under high tensile ratios, this was mainly caused by the roller getting stuck behind the tensile point. However, after processing, the data returned to normal. The stress fluctuation amplitude in the two-layer experimental data is smaller and smoother due to a large tensile force.

The stresses from the single-corner-point tension tend to exceed those from the two-corner-point-fixed tension within the stretch range of approximately 2.25 (as shown in Figure 6), but the stresses from the two-corner-point-fixed tension grow larger as the stretch increases continually. This is primarily due to the fact that the data from the single-corner-point tension were only obtained under quasistatic condition without relaxation, whereas the tensile forces from the two-corner-point-fixed equibiaxial tension are acquired after stretching the specimen under quasistatic conditions ($\dot{\lambda} \approx 5 \times 10^{-4} s^{-1}$) and relaxing for about 10 minutes. When the stretch increases in the two-corner-point-fixed tension, the tensile forces increase abnormally due to significant distortion occuring near the corner of the specimen.

3.2. Fitting from Experimental Data. The model parameters can be obtained through fitting the experimental data. Because the measured tensile force of a two-layer specimen subjected to single-corner-point tension is more stable, three typical models were fitted using this data, as depicted in Figure 7. The residuals obtained from curve fitting were assessed using the root mean square (*RMS*) as defined in Equation (12), where N denotes the number of data points, Y_{g} represents the generated equibiaxial tensile stress, and Y_{m} corresponds to the actual measured stress.

$$\mathrm{RMS} = \sqrt{\frac{1}{N}\sum_{i=1}^{N}\left\{\left(Y_g(i) - Y_m(i)\right)^2\right\}}. \quad (12)$$

The model parameters and RMS are listed in Table 1, along with the results obtained from the two-corner-point-fixed tension test for comparison purposes. Generally speaking, a large number of model parameters will lead to higher accuracy in fitting. According to the RMS, the first-order Mooney-Rivlin model with only two parameters has limited applicability within a narrow range of stretch. On the other hand, models such as Yeoh and Ogden with more parameters exhibit good fitting accuracy over a wider range and can be employed for larger deformation analyses (about $\lambda > 2$). Among these models, the three-parameter Yeoh model achieves even higher fitting accuracy than the four-parameter Ogden model. The overall fitting accuracy of the model is lower due to the larger fluctuation of experimental data from the two-corner-point-fixed tension, despite the RMS values being close among all three models.

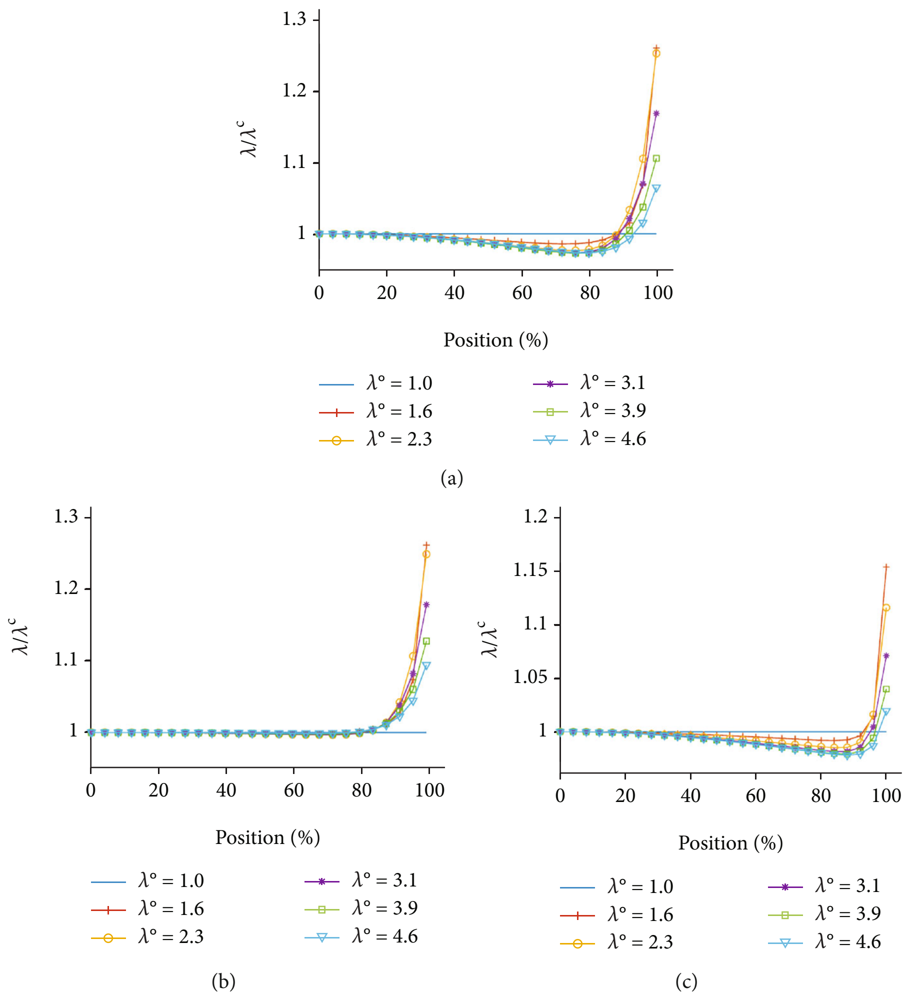

FIGURE 9: Comparison of the axial deformation in different equibiaxial planar tension tests: (a) two-corner-point-fixed tension, (b) single-corner-point tension, and (c) multipoint tension with two- corner-point-fixed.

3.3. Analysis of Simulation Results. Figure 8 presents three strain contour maps, which reveal that the strains are nonuniform near the tensile points in equibiaxial planar tension. Moreover, some areas between two corner tensile points exhibit no deformation in two-corner-point-fixed tension (Figure 8(a)). Although increasing the number of tensile points in Figure 8(c) leads to an overall increase in deformation, it fails to eliminate the stress shielding phenomenon near the corner. In contrast, the deformation in single-corner-point tension (Figure 8(b)) is more uniformly distributed across most rectangular areas around the center, with the exception of a small region near the tensile points (including the corner).

3.3.1. Strain along the Symmetry Axis. The nonuniformity of deformation during equibiaxial tension will have an impact on the accuracy of the derived strain used to determine stress-strain behavior, ultimately resulting in lower experimental accuracy. A series of observation points were assigned along the symmetry axis, and the positions are expressed as a ratio of their geometry position from the center to the length of the unformed specimen ($L_s/2$). The stretch ratio λ^c of the central segment can be selected as a representative value for calculating the stress-strain relationship of the specimen. The ratio of λ^c to the external stretch ratio, λ^o, calculated from the tensile point can serve as an indicator of tensile efficiency η^λ. In this paper, a maximum displacement up to $\lambda^o = 4.6$ (equivalent to 180 mm) was utilized for the three tension tests. λ^c is then taken to normalize the stretch ratios from observation points, i.e., λ/λ^c. This allowed for the derivation of relative axial strains in different equibiaxial planar tensions, as shown in Figure 9.

TABLE 2: Summary of the performance of various equibiaxial planar tension tests.

Tension method	Two-corner-point-fixed	Single-corner-point	Multipoint
Stress error (%) $\lambda = 4$	6.2	2.1	4.6
η^λ (%) $\lambda^O = 4.6$	93.9	91.4	98.1

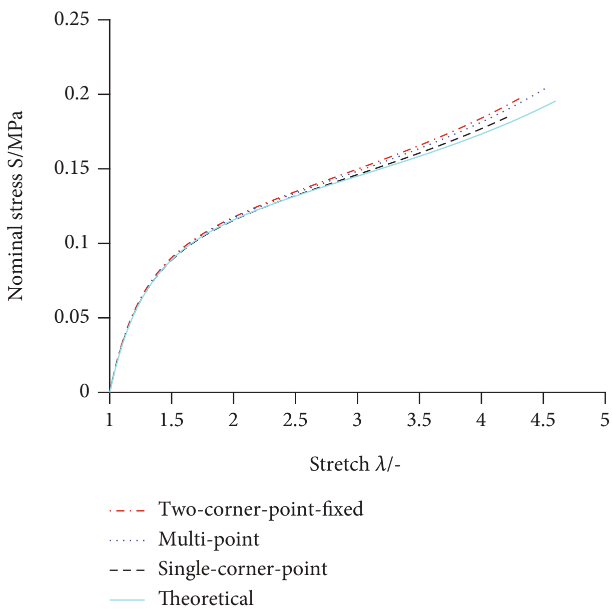

Figure 10: Comparison between the stress-strain curves obtained from the simulation and theory.

The figure illustrates that the stretch ratios vary at different positions along the axis, with a slight decrease in amplitude of no more than 5% from the beginning. However, after exceeding about 80% of the overall axial length, the stretch ratios gradually increase due to tensile forces acting on the tensile point and reach their maximum at the point. The maximum strain at the tensile point will decrease due to the increasing number of tensile points (Figure 9(c)), which is beneficial for improving the tensile efficiency and reducing rig volume. The tensile efficiencies η^{λ} (at $\lambda^{O} = 4.6$) for the three planar tensions are tabulated in Table 2.

The deformation of the single-corner-point tension (Figure 9(b)) is overall more uniform, with strain fluctuation amplitude remaining below 1% for 85% of the axial length. In contrast, in the two-corner-point-fixed tension and the multipoint tension (Figures 9(a) and 9(c)), the same amplitude is observed within approximately 40% and 50% of the axial length, respectively. Therefore, it can be asserted that a more uniform strain can be achieved by utilizing sampling data within the aforementioned range of the specimen during tension testing. The same conclusions can also be obtained when the tensile point does not pass through the symmetry axis, but the variation trend of the strain will be opposite.

3.3.2. Stress-Strain Relationship. Sum up the tensile forces at each tensile point, including the force component near or at the corner point, and then calculate the nominal stress using Equation (11). By selecting λ^{c} as the strains of the specimen, the stress-strain relationships of the hyperelastic membrane under different tensions can be derived (see Figure 10).

It is evident that the stress-strain curves obtained from the three typical equibiaxial planar tension tests agree with theoretical calculations, and any discrepancies will increase as the stretch ratio rises due to distortion. Among them, the simulation results of the stress-strain relationship in the single-corner-point tension are the closest to the theoretical values due to relatively uniform overall deformation, with a stress error of approximately 2.1% at $\lambda = 4$. The highest tensile efficiency ($\eta^{\lambda} = 98.1$) is achieved through multipoint tension with two-corner-point-fixed at $\lambda^{O} = 4.6$, as this method increases the number of tensile points and ensures more complete specimen deformation. The stress errors (at $\lambda = 4$) are also listed in Table 2.

4. Conclusion

Equibiaxial planar tension tests are widely used as test methods for characterizing various hyperelastic membrane materials, but the accuracy of these methods has never been discussed. This article presents a multifunctional equibiaxial planar tension test rig for carrying out the single-corner-point equibiaxial planar tension test of hyperelastic EAP membrane material. The experimental results were compared with those of the two-corner-point-fixed planar tension test. It is found that the stress-strain curve from the single-corer-point tension is more smooth, especially at large deformation.

By means of finite element software, namely, ABAQUS, the two test methods were modeled, and the simulation for the multipoint tension with two-corner-point-fixed was carried out. The obtained stress-strain curves were compared with that from the theoretical calculation. The simulation reveals that the single-corner-point tension can effectively avoid the stress shielding phenomenon near the corner of the specimen and yield a stress-strain curve that is closer to the theoretical one and agrees with the experimental result.

Uniformity in deformation is believed to affect the experimental accuracy. Therefore, the deformation of the above-mentioned three tension tests was also analyzed. In this paper, the ratio of the stretch ratio near the center of the specimen to the external stretch ratio calculated from the tensile point was defined as tensile efficiency, which also indicates the overall deformation degree. It was found through a calculation that increasing the tensile points can obtain higher tensile efficiency, which also helps reduce the force error and design a compact test rig.

The conclusions derived in this paper can provide good guidance for the design of equibiaxial planar tension test rigs and a reference for the analysis of experimental accuracy. Although this paper focuses on the three typical equibiaxial planar tension methods, it can easily be extrapolated to other types of equibiaxial planar tension tests.

Data Availability

Data will be available upon necessary request.

Conflicts of Interest

The authors declare that they have no conflicts of interest.

Acknowledgments

The authors appreciate the financial support from the Natural Science Research Projects in Jiangsu Universities of China (Jiangsu Provincial Department of Science and Technology, Grant No. 18KJA4600050), High-Level Talent Project of "Six Talent Peaks" in Jiangsu Province of China (Grant No. GDZB-024), Open Project of National Key Laboratory of Robotics of China (Grant No. 2018-016), Doctoral Fund of Nanjing Vocational College of Information Technology of China (Grant No. YB20160201). The authors sincerely thank Professor Hua-ming Wang of Nanjing University of Aeronautics and Astronautics for his constructive suggestion during manuscript preparation. The related manuscript was already published as a printer based on the link https://assets.researchsquare.com/files/rs-402426/v1_covered.pdf?c=1631861925.

References

[1] G. Li, X. Chen, F. Zhou et al., "Self-powered soft robot in the Mariana Trench," *Nature*, vol. 591, no. 7848, pp. 66–71, 2021.

[2] T. Li, Z. Zou, G. Mao et al., "Agile and resilient insect -scale robot," *Soft Robotics*, vol. 6, no. 1, pp. 133–141, 2019.

[3] Y. F. Chen, S. Xu, Z. Ren, and P. Chirarattananon, "Collision resilient insect-scale soft-actuated aerial robots with high agility," *IEEE Transactions on Robotics*, vol. 37, no. 5, pp. 1752–1764, 2021.

[4] Y. L. Zhu, C. Hua, X. F. Su, L. B. Geng, Z. Q. Hu, and H. J. Su, "Investigation on flexible pressure sensor array and signal acquisition system," *Transactions of the Chinese Society of Agricultural Machinery*, vol. 51, no. 8, 2020.

[5] G. H. Liang, *Design and Mechanical Modeling of Distributed Flexible Tactile Sensor Array*, Zhejiang University, Hangzhou, 2017.

[6] Z. P. Wang, X. T. Fu, and L. X. Ma, "Numerical mechanical analysis of filled rubber under different deformation states based on a new hyperelastic constitutive model," *Materials Science Forum*, vol. 1032, pp. 15–22, 2021.

[7] Z. Liao, J. Yang, M. Hossain, G. Chagnon, L. Jing, and X. Yao, "On the stress recovery behaviour of ecoflex silicone rubbers," *International Journal of Mechanical Sciences*, vol. 206, article 106624, 2021.

[8] A. Ricker, N. H. Krger, and P. Wriggers, "Comparison of discontinuous damage models of Mullins-type," *Archive of Applied Mechanics*, vol. 91, no. 10, pp. 4097–4119, 2021.

[9] K. Genovese, L. Lamberti, and C. Pappalettere, "Mechanical characterization of hyperelastic materials with fringe projection and optimization techniques," *Optics & Lasers in Engineering*, vol. 44, no. 5, pp. 423–442, 2006.

[10] M. Sasso, G. Palmieri, G. Chiappini, and D. Amodio, "Characterization of hyperelastic rubber-like materials by biaxial and uniaxial stretching tests based on optical methods," *Polymer Testing*, vol. 27, no. 8, pp. 995–1004, 2008.

[11] S. H. Li, H. M. Jia, M. D. Li, Z. M. Qin, and H. L. Chen, "Theory and experimenting method of hyperelastic material constitutive model," *China Elastomerics*, vol. 21, no. 1, pp. 58–64, 2011.

[12] K. Miller, *Testing Elastomer for Hyperelastic Material Models in Finite Element Analysis*, Axel Products Testing and Analysis Report, 2000.

[13] J. Park, Y. Kim, J. W. Yoon, H. So, J. Lee, and S. Ko, "Finite element modeling and durability evaluation for rubber pad forming process," *IOP Conference Series Materials Science and Engineering*, vol. 651, no. 1, article 012096, 2019.

[14] Y. Lanir and Y. C. Fung, "Two-dimensional mechanical properties of rabbit skin-I. Experimental system," *Journal of Biomechanics*, vol. 7, no. 1, pp. 29–34, 1974.

[15] M. Zemánek, J. Burša, and M. Děták, "Biaxial tension experiments with soft tissues of arterial wall," *Engineering Mechanics*, vol. 16, no. 1, pp. 3–11, 2009.

[16] L. Chevalier and Y. Marco, "Tools for multiaxial validation of behavior laws chosen for modeling hyper- elasticity of rubber-like materials," *Polymer Engineering & Science*, vol. 42, no. 2, 2002.

[17] J. W. Fox, *Electromechanical Characterization of the Static and Dynamic Response of Dielectric Elastomer Membranes, [Ph.D. thesis]*, Virginia Polytechnic Institute and State University, Blacksburg, 2007.

[18] H. A. Luo, H. M. Wang, and Y. P. You, "Experimental methods of equiaxial tension of hyperelastic membrane and corresponding simulations," *Journal of South China University of Technology*, vol. 39, no. 4, pp. 56–61, 2011.

[19] Y. Obata, S. Kawabata, and H. Kawai, "Mechanical properties of natural rubber vulcanizates in finite deformation," *Journal of Polymer Science Part A-2: Polymer Physics*, vol. 8, no. 6, pp. 903–919, 1970.

[20] J. P. Blatz and W. L. Ko, "Application of finite elastic theory to the deformation of rubbery materials," *Journal of Rheology*, vol. 6, no. 1, pp. 223–252, 1962.

[21] J. P. Blatz, "Application of finite elastic theory to the behavior of rubber-like materials," *Rubber Chemistry & Technology*, vol. 36, no. 5, pp. 1459–1496, 1963.

[22] N. T. Jacobs, D. H. Cortes, E. J. Vresilovic, and D. M. Elliott, "Biaxial tension of fibrous tissue: using finite element methods to address experimental challenges arising from boundary conditions and anisotropy," *Journal of Biomechanical Engineering*, vol. 135, no. 2, article 021004, 2013.

[23] B. C. Duncan, *Experiment Methods for Determining Hyperelastic Properties of Flexible Adhesives*, National Physical Laboratory, American, 1999.

[24] E. Jiménez-Ruiz, F. Somovilla-Gómez, S. Iñiguez-Macedo, C. Berlanga-Labari, M. Corral-Bobadilla, and R. Lostado-Lorza, *A Proposed Methodology for Calculating the Rigid Body Natural Frequencies of EPDM Rubber Fixed Supports with the Finite Element Method (FEM)*, Springer, Cham, 2020.

[25] R. Escribano, R. Lostado, F. J. Martínez-de-Pisón, A. Pernía, and E. Vergara, "Modelling a skin-pass rolling process by means of data mining techniques and finite element method," *Journal of Iron and Steel Research International*, vol. 19, no. 5, pp. 43–49, 2012.

[26] H. Luo, Y.-l. Zhu, H.-f. Zhao, and J.-j. Zhang, "Analysis of equibiaxial tension tests for hyperelastic EAP film," 2021, https://assets.researchsquare.com/files/rs-402426/v1_covered.pdf?c=1631861925.

[27] H. M. Raheem and A. M. Al-Mukhtar, "Experimental and analytical study of the hyperelastic behavior of the hydrogel under unconfined compression," *Procedia Structural Integrity*, vol. 25, pp. 3–7, 2020.

[28] H. M. Raheem and A. M. Al-Mukhtar, "Experimental investigation of the effects of infusing a foam into hydrogels on the

hyperelastic coefficients," *Material Design & Processing Communications*, vol. 3, 2021.

[29] M. Mooney, "A theory of large elastic deformation," *Journal of Applied Physics*, vol. 11, no. 9, pp. 582–592, 1940.

[30] R. S. Rivlin and A. G. Thomas, "Large elastic deformations of isotropic materials. Viii. Strain distribution around a hole in a sheet," *Philosophical Transactions of the Royal Society of London. Series A, Mathematical and Physical Sciences*, vol. 243, no. 865, pp. 289–298, 1951.

[31] O. H. Yeoh, "Characterization of elastic properties of carbon-black-filled rubber vulcanizates," *Rubber Chemistry and Technology*, vol. 63, no. 5, pp. 792–805, 1990.

[32] R. W. Ogden, "Large deformation isotropic elasticity-on the correlation of theory and experiment for incompressible rubberlike solids," *Proceedings of the Royal Society of London*, vol. 326, no. 1567, pp. 565–584, 1972.

[33] S. Íñiguez-Macedo, R. Lostado-Lorza, R. Escribano-García, and M. Á. Martínez-Calvo, "Finite element model updating combined with multi-response optimization for hyper-elastic materials characterization," *Materials*, vol. 12, no. 7, p. 1019, 2019.

[34] R. L. Lorza, F. J. Ascacibar, R. Fernandez, and J. F. Ceniceros, "Using genetic algorithms to optimize the material behaviour model in finite element models of processes with cyclic loads," *The Journal of Strain Analysis for Engineering Design*, vol. 46, no. 2, pp. 143–159, 2011.

[35] M. Illera, R. Lostado, R. Fernandez Martinez, and B. J. Mac Donald, "Characterization of electrolytic tinplate materials via combined finite element and regression models," *Journal of Strain Analysis for Engineering Design*, vol. 49, no. 6, pp. 467–480, 2014.

[36] A. M. Al-Mukhtar, "Mixed-mode crack propagation in cruciform joint using Franc2D," *Journal of Failure Analysis and Prevention*, vol. 16, no. 3, pp. 326–332, 2016.

[37] H. A. Luo, H. M. Wang, and Y. L. Zhu, "A nonlinear hyperelastic model for dielectric electroactive polymer materials," *Journal of Mechanical Engineering*, vol. 52, no. 14, pp. 73–78, 2016.